

University of Groningen

## Piezoelectric properties of PZT by an ethylene glycol-based chemical solution synthesis

van der Veer, Ewout; Noheda, Beatriz; Acuautla, Mónica

*Published in:*  
Journal of Sol-Gel Science and Technology

*DOI:*  
[10.1007/s10971-021-05651-6](https://doi.org/10.1007/s10971-021-05651-6)

**IMPORTANT NOTE: You are advised to consult the publisher's version (publisher's PDF) if you wish to cite from it. Please check the document version below.**

*Document Version*  
Publisher's PDF, also known as Version of record

*Publication date:*  
2021

[Link to publication in University of Groningen/UMCG research database](#)

*Citation for published version (APA):*

van der Veer, E., Noheda, B., & Acuautla, M. (2021). Piezoelectric properties of PZT by an ethylene glycol-based chemical solution synthesis. *Journal of Sol-Gel Science and Technology*, 100, 517–525.  
<https://doi.org/10.1007/s10971-021-05651-6>

### Copyright

Other than for strictly personal use, it is not permitted to download or to forward/distribute the text or part of it without the consent of the author(s) and/or copyright holder(s), unless the work is under an open content license (like Creative Commons).

The publication may also be distributed here under the terms of Article 25fa of the Dutch Copyright Act, indicated by the "Taverne" license. More information can be found on the University of Groningen website: <https://www.rug.nl/library/open-access/self-archiving-pure/taverne-amendment>.

### Take-down policy

If you believe that this document breaches copyright please contact us providing details, and we will remove access to the work immediately and investigate your claim.

*Downloaded from the University of Groningen/UMCG research database (Pure): <http://www.rug.nl/research/portal>. For technical reasons the number of authors shown on this cover page is limited to 10 maximum.*



# Piezoelectric properties of PZT by an ethylene glycol-based chemical solution synthesis

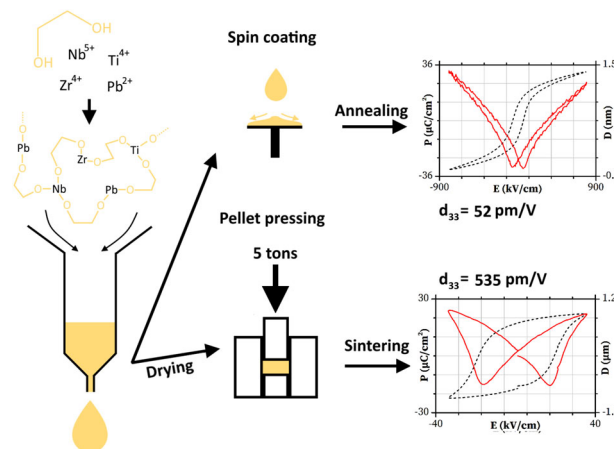
Ewout van der Veer<sup>1</sup> · Beatriz Noheda<sup>1</sup> · Mónica Acuautila<sup>1,2</sup>

Received: 30 June 2021 / Accepted: 19 September 2021 / Published online: 29 October 2021  
© The Author(s) 2021

## Abstract

We have investigated a water-stable sol–gel method based on ethylene glycol as a solvent and bridging ligand for the synthesis of ferroelectric lead zirconate titanate in bulk and thin film forms. This method offers lower toxicity of the solvent, higher stability toward atmospheric moisture and a simplified synthetic procedure compared to traditional sol–gel methods. However, the piezoelectric properties of products produced using this method have yet to be systematically studied. We have measured the ferroelectric and piezoelectric properties and compared them to existing literature using different synthesis techniques. Ceramic pellets of Nb-doped lead zirconate titanate (PNZT) in the tetragonal phase were produced with high density and good piezoelectric properties, comparable to those reported in the literature and those found in commercial piezoelectric elements. In addition, a nine-layer thin film stack was fabricated by spin coating onto platinumized silicon substrates. The films were crack-free and showed a perovskite grain structure with a weak (111) orientation. Piezoelectric measurements of the film showed a piezoelectric coefficient comparable to literature values and good stability toward fatigue.

## Graphical Abstract



**Keywords** Ferroelectric · Sol–gel · PZT · Ethylene glycol · CSD

✉ Mónica Acuautila  
m.i.acuautila.meneses@rug.nl

<sup>1</sup> Zernike Institute for Advanced Materials, Nijenborgh 4, 9747AG Groningen, The Netherlands

<sup>2</sup> Engineering and Technology Institute Groningen, Nijenborgh 4, 9747AG Groningen, The Netherlands

## Highlights

- Pellets and thin films of PZT were produced using an ethylene glycol-based CSD method.
- Ferroelectric and piezoelectric properties of these materials were measured and compared to literature.
- These properties rival literature values.

## 1 Introduction

Sol–gel methods are commonly used for the fabrication of oxide materials with a wide range of functionalities [1–5]. These methods involve the synthesis of a precursor solution (known as ‘sol’) containing oligomeric chains of metal ions and oxygen atoms. Treatment of the sol, for example by the addition of water or by heating, causes the formation of a continuous metal–oxygen network, leading to gelation of the sol. The sol may be processed into a variety of products, such as bulk powders (by simply heating the gel), thin films (by deposition of the sol onto a substrate, *e.g.* by spin coating) or a multitude of other forms [4, 6]. Employing a sol–gel-type synthesis for the production of oxide materials facilitates the control of composition and doping, making high homogeneity and short fabrication cycles possible [4]. Furthermore, when used to fabricate thin films, it can give rise to smooth films covering a large surface area with a wide range of film thicknesses up to several micrometers.

One material which has been produced using a sol–gel method is the well-known lead zirconate titanate solid solution ( $\text{PbZr}_{1-x}\text{Ti}_x\text{O}_3$ , also known as PZT) [7, 8], which is ferroelectric and, thus, piezoelectric, allowing for its use as sensors and actuators [9]. The PZT composition with  $x = 0.48$  lies at a phase boundary between two different crystal structures with tetragonal (for Ti-rich compositions) and rhombohedral (for Zr-rich compositions) symmetries, where monoclinic structures have been observed [10]. At this boundary, known as the morphotropic phase boundary (MPB), the piezoelectric coefficients are maximized [11]. The piezoelectric parameters of PZT can be further improved through chemical doping with elements such as niobium ( $\text{PbNb}_y(\text{Ti}_x\text{Zr}_{1-x})_{1-y}\text{O}_3$  or PNZT) [12, 13].

Traditional sol–gel methods used for the production of thin films of PZT, first reported in the seminal work by Budd *et al.* [7], make use of the highly toxic 2-methoxyethanol as a solvent and alkoxides and acetates as the precursors for lead, zirconium, and titanium. These methods rely on hydrolysis and condensation reactions of the alkoxide precursors to form a polymeric network of metal–oxygen–metal bonds. These methods use water for the initiation of the hydrolysis reaction. Hence, sols produced using such an approach tend to be sensitive to the presence of water [4]. As a result, these sols require storage and processing in an oxygen-free and water-free environment, such as a glovebox.

A simplified sol–gel method was developed by Yi and Sayer [5], which is based on the use of acetic acid to chelate

the metal ions. The resulting metal alkoxide acetates are dissolved in a water-based solution. This method does not require rigorous water-free storage or refluxing/distillation procedures, which is the case for the conventional sol–gel method. Nevertheless, the species present in the solution still depend on the concentration of water.

More recently, there has been an interest in the development of chemical solution deposition (CSD) methods that are not based on hydrolysis–condensation reactions, instead relying on different types of reactions. These include the well-known Pechini process [2, 4], which uses citric acid as a chelating agent and ethylene glycol as a bridging molecule between metal ions; nonaqueous sol–gel methods [14], in which metal–oxygen–metal bonds are formed without hydrolysis and condensation; and the citrate method [2, 4]. A final example of such a CSD method is based on only ethylene glycol as a bridging ligand and common alkoxides and acetates as reagents. This method was reported to be nontoxic, more stable to atmospheric moisture, able to provide thicker single layers and offer a more straightforward synthesis procedure [2, 15]. However, the ferroelectric and piezoelectric properties of materials produced using this method have not been systematically compared to those using other synthesis methods. It is important for practical applications of this method to ascertain that the increased organic content of the sol does not degrade these properties.

We aim to fill this gap by measuring the piezoelectric and ferroelectric properties of bulk and thin film products of the ethylene glycol-based CSD method and comparing them to existing literature. We show that multilayer stacks of thin films can be produced without cracks or parasitic phases by controlling the deposition and heat treatment procedures. Thus, despite the presence of a large amount of organic material in the as-deposited film, which can reduce film quality, the piezoelectric behavior of the bulk and thin film products are comparable to reported values for films of similar characteristics.

## 2 Materials and methods

### 2.1 Sol synthesis

7.5 g of freeze-dried lead acetate ( $\text{Pb}(\text{CH}_3\text{COO})_2$ ,  $\text{PbAc}_2$ , 23 mmol, 10 mol% excess,  $\geq 99\%$ , Sigma Aldrich) and 9.4 mL ethylene glycol ( $(\text{CH}_2\text{OH})_2$ , EG) were added to a three-necked flask under a 0.5 L/min argon flow. An excess of lead acetate

was used to compensate for losses due to evaporation and diffusion during the heat treatment steps. The suspension was heated to 90 °C while stirring to dissolve the solids, then to 110 °C to expel any remaining water from the solution. The sol was subsequently cooled to 90 °C. 2.857 mL of titanium isopropoxide ( $\text{Ti}(\text{OCH}(\text{CH}_3)_2)_4$ , 2.743 g, 9.65 mmol, 97%, Sigma Aldrich), 0.210 mL niobium ethoxide ( $\text{Nb}(\text{OCH}_2\text{CH}_3)_5$ , 0.266 g, 0.836 mmol, 99.95%, Sigma Aldrich) and 4.686 mL of a 70 wt.% solution of zirconium n-propoxide in 1-propanol ( $\text{Zr}(\text{OCH}_2\text{CH}_2\text{CH}_3)_4$ , 3.425 g  $\text{Zr}(\text{OCH}_2\text{CH}_2\text{CH}_3)_4$ , 10.5 mmol, Sigma Aldrich) were dissolved in 6.1 mL 1-propanol under inert atmosphere. The Ti/Nb/Zr solution was added to the lead sol slowly limiting exposure to air. Some precipitate formed upon addition. A further 15.7 mL of EG was added, yielding 30 mL of solution at a concentration of metal ions of 1.5 M with a nominal composition of  $\text{Pb}_{1.1}\text{Nb}_{0.04}(\text{Zr}_{0.52}\text{Ti}_{0.48})_{0.96}\text{O}_3$ . The suspension was stirred at 90 °C until all precipitate had redissolved. The sol was cooled to room temperature and 4 vol.% formamide ( $\text{HCONH}_2$ ,  $\geq 99\%$ , Sigma Aldrich) was added as a drying control chemical additive to limit the formation of cracks in the films [1]. A second sol was made in the same way, using a 0% excess of lead precursor. This sol was used for the preparation of bulk PNZT (see below).

A separate lead oxide (PbO) sol was fabricated by dissolving 9.76 g of freeze-dried lead acetate ( $\text{Pb}(\text{CH}_3\text{COO})_2$ ,  $\text{PbAc}_2$ , 23 mmol, 10 mol% excess,  $\geq 99\%$ , Sigma Aldrich) in 30 mL of ethylene glycol ( $(\text{CH}_2\text{OH})_2$ , EG) while stirring to a final concentration of 1 M.

## 2.2 Substrate preparation

The substrates used for deposition of the PNZT sol were prepared from a (001) oriented silicon wafer without thermal oxide (Ted Pella) diced into  $1 \times 1$  cm squares. The silicon substrates were cleaned ultrasonically in acetone, demineralized water and ethanol for 10 min each. The substrates were subsequently blow-dried using compressed air and loaded into a Kurt J. Lesker sputtering system. The substrates were  $\text{O}_2$  plasma cleaned (0.15 mbar, 200 W, 5 min) after which a titanium adhesion layer of 5 nm was DC sputtered (200 W, 0.2 nm/s) without breaking the vacuum. Subsequently, a 100-nm-thick electrode of platinum was DC sputtered (200 W, 1.61 nm/s) onto the adhesion layer. The full electrode stack was annealed in a box furnace in air (450 °C, 90 min, ramp rate 14.2 °C/s).

## 2.3 Deposition procedure and heat treatment

The platinized silicon substrates prepared as described above were again cleaned ultrasonically in acetone, demineralized water, and ethanol for 10 min each. The substrates were blow dried using compressed air and UV/ $\text{O}_3$  treated in an Ossila UV ozone cleaner for 10 min to remove any

residual organic contamination from the surface. The substrates were immediately placed in the center of the vacuum chuck of a spin coater. Seventy-five microliters of the 1.5 M sol was deposited onto the substrates. The spin coater was subsequently ramped up to the desired speed at 1000 rpm/s. It was held at this speed for 30 s, then slowed to a stop at 1000 rpm/s. The film was then placed on a hotplate at 230 °C for drying. Additional layers were deposited after drying for the production of multilayer films. After the deposition of up to three layers, the films were pyrolyzed at 380 °C on the hotplate and annealed by placing them in a preheated box furnace at 650 °C for 10 min. Multilayer stacks of up to nine single deposited layers were produced, for which pyrolysis and annealing steps were performed every third layer. Multiple annealed layers are required to prevent the formation of leakage paths through the film. A  $4 \times 4$  grid of circular top electrodes of 100 nm of platinum was sputter deposited onto the films using a hard mask.

## 2.4 Pellet preparation

For the preparation of bulk pellets of PNZT, the sol without an excess of lead was stirred and heated at 230 °C on a hotplate. Some of the resulting gel was used for thermogravimetric analysis (TGA) and differential thermal analysis (DTA). The remaining gel was heated in a box furnace to 450 °C for 1 h to remove the organic groups. The resulting powder was ball milled for 30 min and heated again to 450 °C for 10 min. The PNZT powder was pressed into 0.48 g pellets with a nominal diameter of 10 mm under a load of 6.4 ton/cm<sup>2</sup> using poly(vinyl alcohol) as a binder. The green body had a density of 5292 kg/m<sup>3</sup>. The pellets were placed on top of a piece of platinum inside an alumina crucible with a mixture of lead zirconate and 10% zirconium dioxide to control the composition of the atmosphere during sintering (Fig. 1) [16]. They were sintered in a box furnace at 1250 °C for 2 h.

## 2.5 Characterization

Grain structures of the films and pellets and film thicknesses were studied using an FEI Nova NanoSEM 650 scanning electron microscope. Grinding and polishing of the pellet before Scanning electron microscopy (SEM) analysis was done using diamond suspension down to 1  $\mu\text{m}$  (Struers company) and colloidal silica suspension down to 40 nm (Struers OP-U). The pellet was then lightly etched in 100 mL of 15% hydrochloric acid with a drop of hydrofluoric acid for 30 s. X-ray diffraction data were collected using a PanAnalytical X'Pert Pro MRD or a Bruker D8 Advance diffractometer (both in Bragg-Brentano geometry) for the films and pellets, respectively. DTA-TGA data was collected in argon from

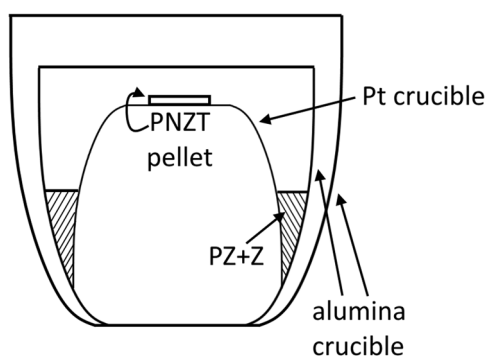


**Fig. 1** Crucible setup used for sintering the PNZT pellet. PZ + Z:  $\text{PbZrO}_3 + 10\% \text{ZrO}_2$

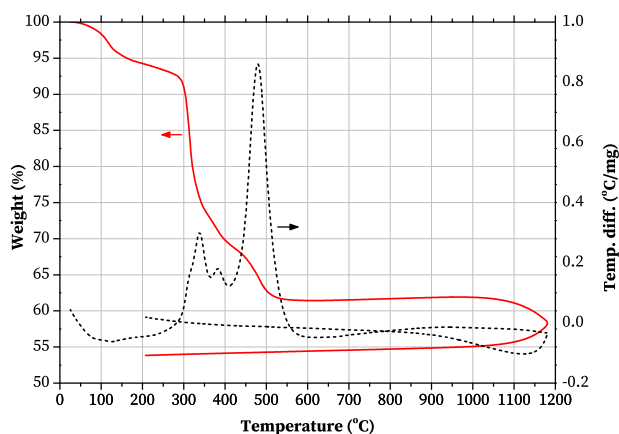


**Fig. 2** DTA and TGA traces of the sol dried at 230 °C

30 °C to 1200 °C at a heating rate of 10 °C/min using a TA instruments SDT 2960 differential scanning calorimeter. Finally, ferroelectric and piezoelectric properties of the films and pellets were measured using a state-of-the-art AixACCT TF analyzer 2000 ferroelectric-piezoelectric characterization system with an AixACCT double beam (films) or a Sios single beam (pellets) interferometer. The use of a double-beam interferometer eliminates the contribution of the bending of the substrate to the measured deformation of the film.

### 3 Results and discussion

Properties of the sol, as well as structural, ferroelectric, and piezoelectric properties of the PNZT films and bulk ceramic pellets have been investigated.

Figure 2 contains plots of the DTA and TGA data collected from the sol dried at 230 °C on a hotplate. Initial weight loss occurs around 100 °C and is likely associated with loss of a small amount of water from the air adhering to the sample, crucible or the inside of the DTA-TGA apparatus. This residual water cannot originate from the sample itself as it was heated to 230 °C prior to the measurement. Further

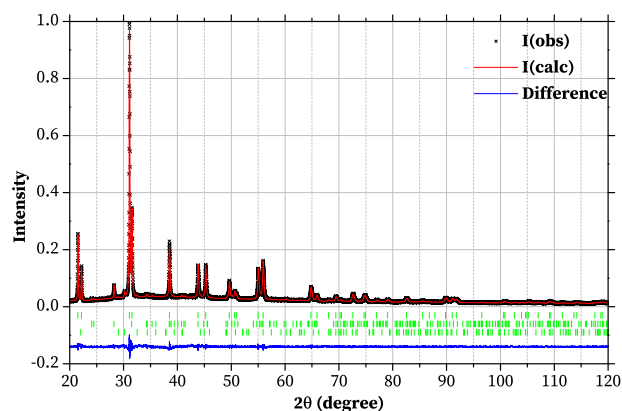


**Fig. 3** X-ray diffraction pattern of the pellet and a fit of the profile. The green indicators show the expected peak positions of (from top to bottom) a rhombohedral PNZT phase, a monoclinic  $\text{ZrO}_2$  phase, and a  $\beta$ -PbO phase, respectively

decomposition of the sample takes place in three steps at 320, 380, and 470 °C. Weight loss above 1000 °C is due to evaporation of lead from the sample. These results closely resemble those found in previous reports on diol-based sol-gel methods [17, 18]. A total weight loss of approximately 38% was observed up to 600 °C.

We found that this type of sol is much less sensitive to the presence of water (for example, from the atmosphere), than traditional sols based on 2-methoxyethanol. These are generally used in an inert atmosphere to prevent undesired gelation. On the contrary, no gelation occurred in the ethylene glycol-based sol for at least a month even after the direct addition of 10% of water to the sol. This opens up possibilities for using the sol in air.

#### 3.1 Bulk

PNZT pellets were produced from the PNZT sol with a 0% excess of lead precursor. The sol was dried at 230 °C and pyrolyzed at 450 °C. Pellets with a nominal diameter of 10 mm were pressed from this powder at 6.4 ton/cm<sup>2</sup> and sintered at 1250 °C for 2 h. After sintering, the pellet had a diameter of 8.52 mm, a thickness of 0.69 mm and a density of 8129 kg/m<sup>3</sup>, 99.3% of the calculated maximum density of 8188 kg/m<sup>3</sup>.

Figure 3 shows an X-ray diffraction pattern of the pellet after sintering at 1250 °C. A LeBail fit of this pattern was made using a combination of a tetragonal PNZT phase (space group  $P4mm$ ), a monoclinic zirconia phase ( $P2_1/c$ ), and an orthorhombic  $\beta$ -PbO phase ( $Pbcm$ ). The latter two phases are minor impurities. Blown-up versions of the (100), (110), and (111) peaks of the pattern are shown in Fig. 4. The nominal composition of the material is at the MPB between the rhombohedral and tetragonal phases, which is known to have the best piezoelectric properties



**Fig. 4** Blow-ups of the **a** (100), **b** (110), and **c** (111) peaks of the pattern in Fig. 3

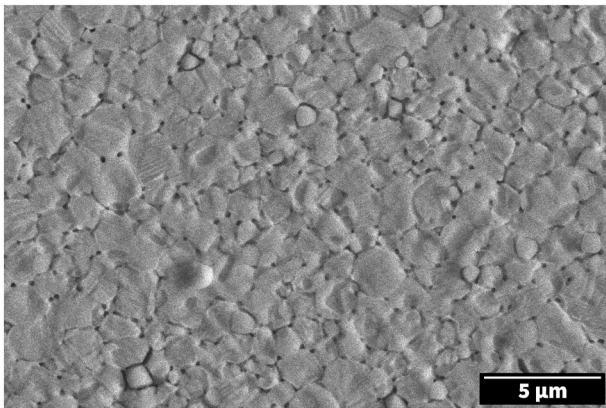
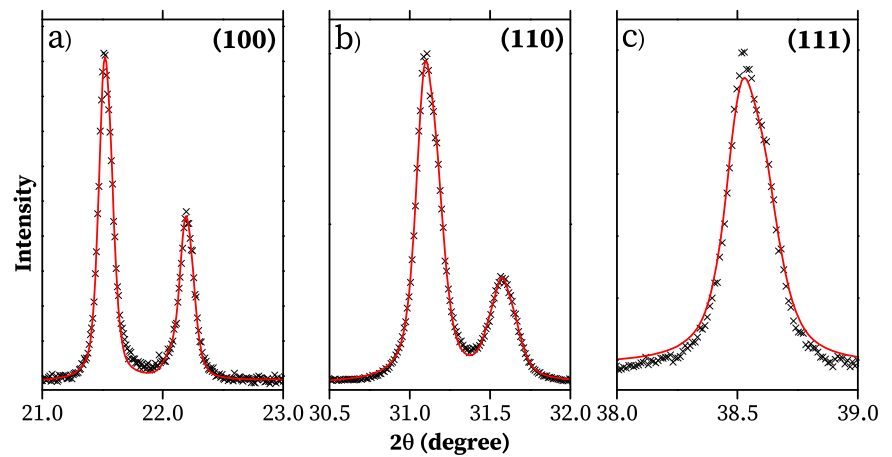


**Fig. 5** Scanning electron microscopy image of a pellet sintered at 1250 °C showing PNZT grains as well as ferroelectric-ferroelastic domains on some of the grains

[10, 11, 19, 20]. However, XRD analysis shows that the material is in fact in the titanium-rich tetragonal phase, due to the formation of a minor zirconia impurity. The process by which this zirconia phase is formed is presently unknown. The formation of this phase as well as its effects on the properties of our products are the topic of ongoing investigation in our group.

SEM of the pellet (Fig. 5) shows a dense grain structure, with visible ferroelastic domains on some of the grains. The diameters of 35 grains were measured, yielding an average grain size of 1.21  $\mu\text{m}$  with a standard deviation of 0.54  $\mu\text{m}$ . The impurity phases observed in the X-ray diffraction pattern are not clearly visible in the micrograph.

The pellet was poled in a silicone oil bath at 100 °C with an electric field of 29 kV/cm for 30 min to align the dipoles in the material. Ferroelectric property measurements of the bulk ceramic pellet were performed with a frequency of 10 Hz, yielding the polarization-electric field hysteresis loops and strain-electric field (“butterfly”) loops expected for a ferroelectric, as displayed in Fig. 6a. The remnant

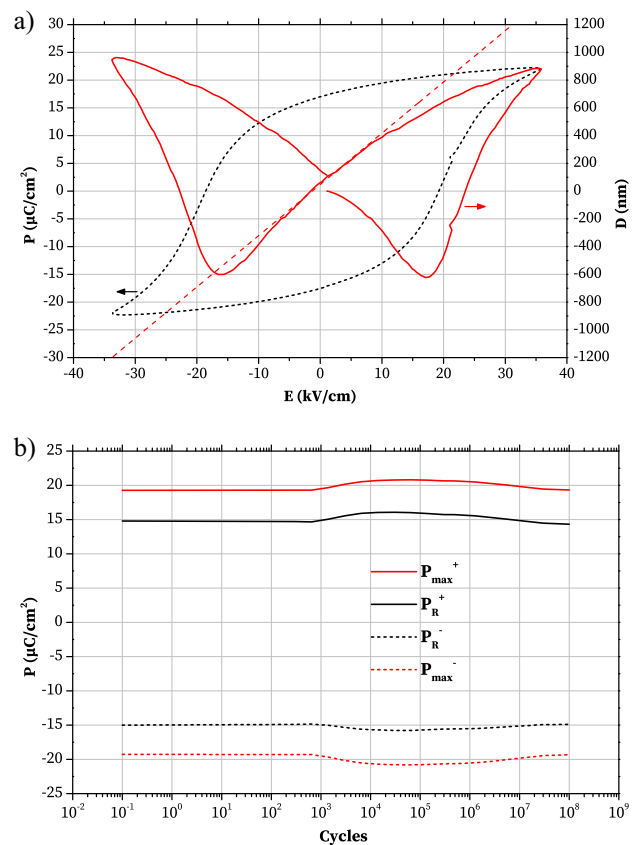


**Fig. 6** **a** Polarization and strain loops of a 0.69 mm thick sol-gel derived PNZT pellet sintered at 1250 °C. The slope of the dashed line is the longitudinal piezoelectric coefficient,  $d_{33} = 535(7)$  pm/V. The slight asymmetry in the strain-field curve is likely due to residual stresses in the sample. **b** Fatigue response of the same pellet showing minimal degradation up to  $10^8$  cycles

polarization measured for this pellet is  $P_r = 17.0 \mu\text{C}/\text{cm}^2$ , the coercive field  $E_c = 19.1 \text{ kV}/\text{cm}$ , and the maximum longitudinal piezoelectric coefficient  $d_{33} = 535 \pm 7 \text{ pm}/\text{V}$ . The piezoelectric coefficient was obtained from the slope of the strain-field curve at zero field. The  $d_{33}$  coefficient

**Table 1** Comparison of the longitudinal piezoelectric coefficient of the PNZT pellet fabricated using the ethylene glycol CSD method with literature values

$d_{33}(\text{pm}/\text{V})$	Doping element	Method	Reference
535(7)	Nb	CSD	This work
500	Commercial	n.a.	[27]
475	Commercial	n.a.	[28]
420	Undoped	Sol-gel	[29]
155	Undoped	Wet chemical	[30]
300	Undoped	Wet chemical	[31]
569	La	Sol-gel	[32]
269	Nd	Sol-gel	[32]
325	La	Wet chemical	[33]
236	$\text{BiFeO}_3/\text{CuO}/\text{BaCu}_{0.5}\text{W}_{0.5}\text{O}_3$	Solid-state	[34]
338	La/Nb	Solid-state	[35]
520	Sr/Nb	Solid-state	[36]
255	Nb	Solid-state	[37]

obtained here is compared to literature values in Table 1. Our PNZT pellet has a piezoelectric coefficient comparable to the best materials found in literature, including commercially available piezoelectric elements. We expect that the ferroelectric and piezoelectric parameters can be further increased by bringing the composition closer to the MPB. Figure 6b shows the fatigue response of the same sample. The polarization shows little to no degradation for at least  $10^8$  cycles. This work shows that the ethylene glycol CSD method is capable of producing a high-quality material despite the simplicity of the method and the presence of a larger amount of organic material in the dried film.

### 3.2 Thin films

A nine-layer PNZT film was produced from the 1.5 M PNZT sol by spinning at 5000 rpm followed by drying on the hotplate, with pyrolysis and annealing steps performed after every third layer. During heat treatment of these films, lead can be lost through evaporation at the film surface and through diffusion into the silicon substrate. This leads to the formation of a layer of lead-deficient pyrochlore phase at the film surface or at the film–electrode interface. An excess of lead precursor can be added to the PNZT sol to compensate for this loss. However, too large an excess can cause the formation of voids in the film due to evaporation of the excess lead species. Therefore, careful control of the excess is required.

To achieve such control, an alternative method was used here. A relatively small excess of lead of 10% was added to the sol, aiming to compensate for diffusion but not for evaporation. In addition, a layer of pure PbO sol was deposited before the

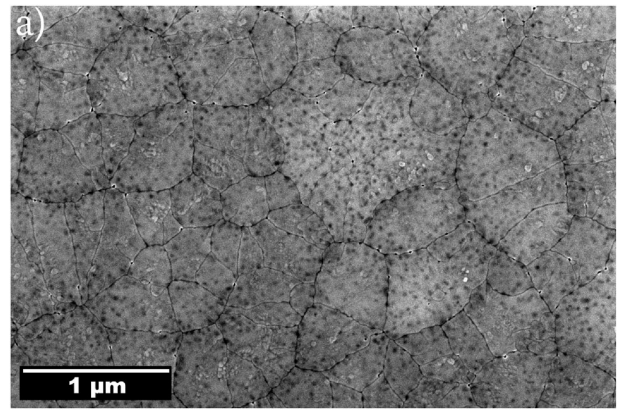


**Fig. 7** Plan-view SEM image of a nine-layer PNZT thin-film stack with a PbO overcoat. The black spots visible on the film are due to pores present primarily at the surface

final pyrolysis step, compensating for evaporation from the film surface (see ref. [21]). The resulting film shows grains with sizes from several hundred nanometers up to  $1\ \mu\text{m}$  (Fig. 7). Black spots on the surface of the film reveal the presence of voids, which are located mostly close to the surface. These voids are presumably caused by the presence of some residual organic material or a very slight excess of lead, but they do not penetrate through the film. Using this procedure, no lead-deficient pyrochlore phase was found and no cracks or leakage paths are visible. These observations show that the combination of a lead excess in the sol with a PbO overcoat is effective at producing crack-free thin films. A columnar grain structure is commonly observed in PZT thin films derived from traditional sol-gel methods based on 2-methoxyethanol, due to bottom-up growth of the grains after heterogeneous nucleation at the film-electrode interface. Such structure is not present in these films, suggesting that the film nucleates more homogeneously throughout, as has been previously observed using diol-based sol-gel methods [18]. This may be the result of the high organic content of the as-deposited films compared to traditional sol-gel-derived films, the relatively high firing temperature and the high heating rate [18].

An X-ray diffraction pattern of the same film is shown in Fig. 8. The pattern shows a pure perovskite PNZT phase with no impurity peaks, except those originating from the platinumized silicon substrate. No peak splitting is observed due to the broadening of the peaks. A small Pt(200) peak is present due to the top electrode, which is not perfectly (111) oriented. The preferential orientation of the PNZT film can be quantified by normalizing the integrated peak intensities with the intensities of the X-ray diffraction patterns of a powdered sample using the following expression [22]:

$$P(h_i k_i l_i) = \frac{I(h_i k_i l_i)}{I^*(h_i k_i l_i)} \frac{I(hkl)}{\sum_{hkl} I^*(hkl)} \quad (1)$$

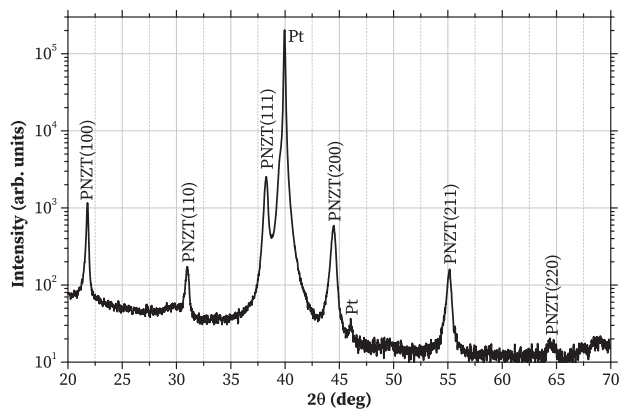


**Fig. 8** XRD pattern of the nine-layer thin film stack

**Table 2** Texture index values of the thin film sample

$\langle h_i k_i l_i \rangle$	$P(h_i k_i l_i)$
$\langle 100 \rangle$	0.25
$\langle 110 \rangle$	0.0086
$\langle 111 \rangle$	0.59
$\langle 200 \rangle$	0.11
$\langle 211 \rangle$	0.020
$\langle 220 \rangle$	0.016

where  $P(h_i k_i l_i)$  is a texture index quantifying the preferred orientation of the sample,  $I(h_i k_i l_i)$  is the intensity in the thin film sample and  $I^*(h_i k_i l_i)$  is the intensity in the powdered sample. The values in Table 2 are obtained using the data in Fig. 8.

A  $\langle 111 \rangle$  orientation is preferred in these films due to the  $\langle 111 \rangle$  texture of the underlying platinum electrode, showing that at least some of the film nucleates heterogeneously at the film-electrode interface. However, it is evident that some of the film nucleates homogeneously, resulting in a decreased  $\langle 111 \rangle$  texture of the film. This is in agreement with the lack of bottom-up growth in the film.

Figure 9a shows the ferroelectric hysteresis loop and strain loop of a nine-layer PNZT thin film stack. A double-beam laser interferometer [23], which corrects for substrate bending to extract the true deformation of the film, was used to collect these loops. The loops were collected by sweeping the potential applied to the top electrode between +800 kV/cm and -800 kV/cm using a triangular waveform at a frequency of 100 Hz. The longitudinal piezoelectric coefficient is extracted from the strain loop by determining its slope at zero applied field. The film showed a remnant polarization of  $10.5 \mu\text{C}/\text{cm}^2$ , somewhat lower than values in literature [17, 18, 24, 25]. The average coercive field was 61.3 kV/cm, similar to the literature [17, 18, 24]. The longitudinal piezoelectric coefficient of  $53 \pm 2 \text{ pm}/\text{V}$  and a maximum deformation of 1.41 nm, or 0.3% of the thickness

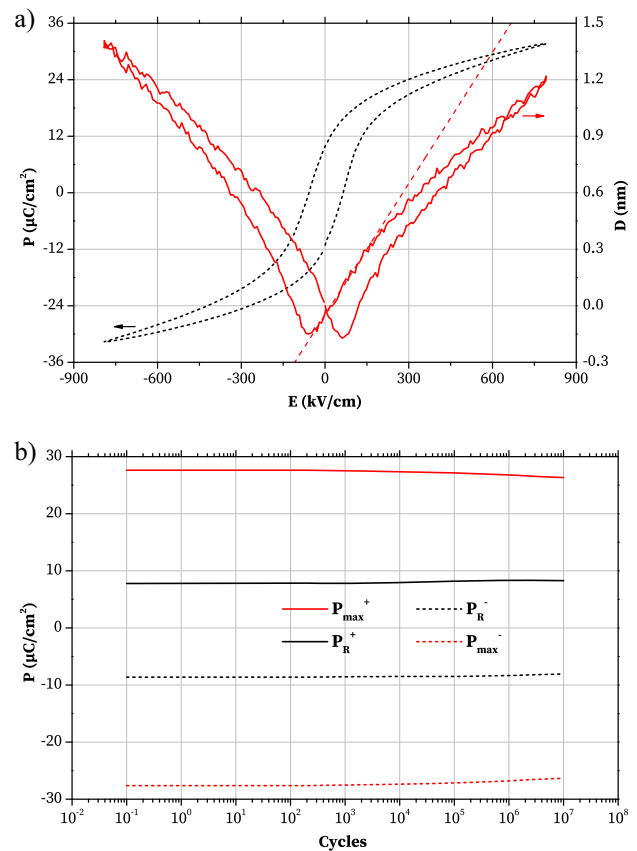


**Fig. 9** **a** Ferroelectric and strain loop of the nine-layer PNZT thin film stack. The longitudinal piezoelectric coefficient is obtained from the slope of the strain loop at zero electric field, as indicated by the red tangent line. **b** Fatigue response of the film up to  $10^7$  cycles

**Table 3** Comparison of the longitudinal piezoelectric coefficient of the PNZT thin film fabricated using the ethylene glycol CSD method with literature values

$d_{33}$ (pm/V)	Production method	Reference
50	CSD	This work
50	Sol-gel	[22]
77	Sol-gel	[38]
200	OMCVD	[39]
400	Sol-gel	[39]
85	Sol-gel	[40]
70–80	Sol-gel	[25]
200	Sol-gel	[24]
25	Sol-gel	[41]
57.6	Sol-gel	[42]
164*	PLD	[43]
106	PLD	[44]

These results are for undoped PZT, unless otherwise noted

PLD pulsed laser deposition

\*1% Nb doping, OMCVD organometallic chemical vapor deposition



of the film, are compared to literature values in Table 3, which displays the wide range of piezoelectric parameter values reported depending on the synthesis technique. Our piezoelectric coefficient is on the low end of this range, but improvements can likely be made. For example, fabrication of thicker films will improve piezoelectric behavior due to reduced clamping from the substrate. Furthermore, our film contains a large number of voids due to the relatively large organic content of the dried film compared to traditional methods. Increasing the density of the film by adjusting the heat treatment procedure will likely improve the piezoelectric coefficient as well.

Figure 9b shows the fatigue response of the film. The film was switched at a frequency of 200 Hz with an electric field amplitude of 114 kV/cm, that is above the coercive field. Ferroelectric hysteresis loops were collected at 3 points/decade with a field amplitude of 800 kV/cm and a frequency of 100 Hz. The film is stable to fatigue for at least  $10^7$  cycles. These results are similar to those reported in the literature (see, e.g., refs. [13, 22, 26]).

## 4 Conclusion

To summarize, a sol–gel method was developed based on ethylene glycol as a solvent and bridging ligand. This sol was used for the production of pellets and thin films of ferroelectric niobium-doped lead zirconate titanate. This sol offers the advantages of a lower toxicity solvent, improved stability during storage, decreased sensitivity to atmospheric moisture and the applicability to the synthesis of both bulk and thin-film products. Furthermore, the synthesis of the sol is less complex than that of traditional, 2-methoxyethanol-based sols. DTA-TGA of the sol shows that decomposition of the gel is finished at 600 °C, with a total weight loss of 38%. Pellets of bulk PNZT were produced, having a density of 99.3% of the theoretical density and small PbO and zirconia impurities. The pellets are in the tetragonal phase with a grain size of  $1.21 \pm 0.54 \mu\text{m}$ . They show good properties with a coercive field of 19.1 kV/cm, a remnant polarization of  $17.0 \mu\text{C}/\text{cm}^2$  and a piezoelectric coefficient of  $535 \pm 7 \text{ pm}/\text{V}$ , comparable to literature values for similar PZT compositions. The pellet shows resistance to fatigue up to at least  $10^8$  cycles.

In addition, a nine-layer stack of PNZT thin films was fabricated from the sol by spin coating with a thickness of 440 nm. An excess of lead was supplied to the thin films to compensate for evaporation and diffusion by combining the addition of an excess of lead precursor to the sol and the application of an overcoat of pure PbO. This method proved effective at suppressing the presence of lead-deficient phases in the stack. The final stack shows a perovskite grain structure with a relatively large number of voids and a weak (111) out-of-plane texture. Ferroelectric and piezoelectric

characterization of the film shows ferroelectric coefficients close to literature values for thin films, with a remnant polarization of  $10.5 \mu\text{C}/\text{cm}^2$ , a coercive field of 61.3 kV/cm, a piezoelectric coefficient of  $52 \pm 2 \text{ pm}/\text{V}$  and a maximum deformation of 0.3% of the thickness of the film. Furthermore, the film shows good stability to fatigue up to  $10^7$  cycles. This sol–gel method provides a safer, more water-stable alternative to traditional sol–gel methods based on 2-methoxyethanol for the fabrication of bulk and thin-film products.

**Acknowledgements** We gratefully acknowledge the invaluable help of Jacob Baas and Henk Bonder in the lab. We thank Miguel Badillo for fruitful discussions.

**Author contributions** EvdV and BN acknowledge financial support by the Ubbo Emmius Fonds of the University of Groningen. MA acknowledges financial support of a NWO-f Fellowship of the Dutch Research Council (NWO).

## Compliance with ethical standards

**Conflict of interests** The authors declare no competing interests.

**Publisher's note** Springer Nature remains neutral with regard to jurisdictional claims in published maps and institutional affiliations.

**Open Access** This article is licensed under a Creative Commons Attribution 4.0 International License, which permits use, sharing, adaptation, distribution and reproduction in any medium or format, as long as you give appropriate credit to the original author(s) and the source, provide a link to the Creative Commons license, and indicate if changes were made. The images or other third party material in this article are included in the article's Creative Commons license, unless indicated otherwise in a credit line to the material. If material is not included in the article's Creative Commons license and your intended use is not permitted by statutory regulation or exceeds the permitted use, you will need to obtain permission directly from the copyright holder. To view a copy of this license, visit <http://creativecommons.org/licenses/by/4.0/>.

## References

- Hench LL, West JK (1990) *Chem Rev* 90:33–72
- Schwartz RW, Schneller T, Waser R (2004) *Comptes Rendus Chim* 7:433–461
- Livage J, Henry M, Sanchez C (1988) *Prog Solid St Chem* 18:259–341
- Danks AE, Hall SR, Schnepf Z (2016) *Mater Horizons* 3:91–112
- Yi GH, Sayer M (1991) *Am Ceram Soc Bull* 70:1173–1179
- Bassiri-Gharb N, Bastani Y, Bernal A (2014) *Chem Soc Rev* 43:2125–2140
- Budd KD, Dey SY, Payne DA (1985) *Br Ceram Soc Proc* 36:107–121
- Kosec M, Malic B, Mandeljc M (2002) *Mat Sci Semicon Proc* 5:97–103
- Muralt P (2000) *J Micromech Microeng* 10:136–146
- Noheda B et al. (1999) *Appl Phys Lett* 74:2059–2061
- Jaffe B, Cook WR, Jaffe HL (1971) *Piezoelectric ceramics*. Academic Press, Cambridge, Massachusetts, United States (Academic Press).

12. Damjanovic D (1998) *Rep Prog Phys* 61:1267
13. Li Q et al. (2017) *J Ceram Sci Technol* 8:519–524
14. Niederberger M (2007) *Acc Chem Res* 40:793–800
15. De-Qing Z, Hong-Shan S, Shao-Jun W, Mao-Sheng C, Xui-Li W (2007) *J Sol-Gel Sci Technol* 41:157–161
16. Kingon AI, Clark BJ (1983) *J Am Ceram Soc* 66:253–256
17. Livage C, Safari A, Klein LC (1994) *J Sol-Gel Sci Technol* 2:605–609
18. Tu YL, Milne SJ (1995) *J Mater Res* 10:3222–3231
19. Noheda B, Gonzalo J, Cross L, Guo R (2000) *Phys Rev B* 61:8687–8695
20. Noheda B et al. (2000) *Phys Rev B* 63:014103
21. Brennecke GL, Ihlefeld JF, Maria JP, Tuttle BA, Clem PG (2010) *J Am Ceram Soc* 93:3935–3954
22. Balma D et al. (2014) *J Am Ceram Soc* 97:2069–2075
23. Pan WY, Cross LE (1989) *Rev Sci Instrum* 60:2701–2705
24. Chen HD et al. (1996) *J Am Ceram Soc* 79:2189–2192
25. Zavala G, Fendler JH, Trolier-McKinstry S (1997) *J Appl Phys* 81:7480–7491
26. Klissurska RD, Tagantsev AK, Brooks KG, Setter N (1997) *J Am Ceram Soc* 80:336–342
27. Hinterstein M et al. (2011) *Phys Rev Lett* 107:077602
28. Xu T-B et al. (2013) *Smart Mater Struct* 22:065015
29. Sharma PK, Ounaies Z, Varadan VV, Varadan VK (2001) *Smart Mater Struct* 10:878–883
30. Choy J-H, Han Y-S, Kim S-J (1997) *J Mater Chem* 7:1807–1813
31. Guiffard B, Troccaz M (1998) *Mater Res Bull* 33:1759–1768
32. Shannigrahi SR, Tay FEH, Yao K, Choudhary RNP (2004) *J Eur Ceram* 24:163–170
33. Sahoo B, Panda PK (2013) *J Adv Ceram* 2:37–41
34. Dong D, Murakami K, Kaneko S, Xiong M (1993) *J Ceram Soc Jpn* 101:1090–1094
35. Singh V, Kumar HH, Kharat DK, Hait S, Kulkarni MP (2006) *Mater Lett* 60:2964–2968
36. Zheng H, Reaney IM, Lee WE, Jones N, Thomas H (2001) *J Eur Ceram* 21:1371–1375
37. Garcia JE, Prez R, Albareda A, Eiras JA (2007) *J Eur Ceram* 27:4029–4032
38. Taylor D, Damjanovic D (2000) *Appl Phys Lett* 76:1615–1617
39. Lefki K, Dormans GJM (1994) *J Appl Phys* 76:1764–1767
40. Ledermann N et al. (2003) *Sens Actuators A* 105:162–170
41. Wang Y et al. (2002) *Appl Phys Lett* 80:97–99
42. Lian L, Sottos NR (2000) *J Appl Phys* 87:3941–3949
43. Nguyen MD et al. (2014) *Ceram Int* 40:1013–1018
44. Goh WC, Yao K, Ong CK (2005) *Appl Phys A* 81:1089–1093